Title
Untangling the Relationship Between AMOC Variability and North Atlantic Upper-Ocean Temperature and Salinity

Journal
Geophysical Research Letters, 48(14)

ISSN
0094-8276

Authors
Chiang, JCH
Cheng, W
Kim, WM
et al.

Publication Date
2021-07-28

DOI
10.1029/2021gl093496

Peer reviewed

Untangling the relationship between AMOC variability and North Atlantic upper-ocean temperature and salinity

J. C. H. Chiang[1], W. Cheng[2,3], W. M. Kim[4], and S. Kim[1]

[1] Department of Geography and Berkeley Atmospheric Sciences Center, University of California, Berkeley, CA, USA.

[2] Cooperative Institute for Climate, Ocean, and Ecosystem Studies, University of Washington, Seattle, WA, USA.

[3] NOAA/Pacific Marine Environmental Laboratory, Seattle, WA, USA.

[4] Climate and Global Dynamics Laboratory, National Center for Atmospheric Research, Boulder, CO, USA.

Corresponding author: John Chiang (jch_chiang@berkeley.edu)

Key Points:

- Maximum Covariance Analysis reveals two modes that separate cause-and-effect between AMOC and North Atlantic T/S in a control simulation
- The two modes effectively span the temporal behavior of AMOC variability as represented by the AMOC maximum streamfunction index
- Analysis of simulation with oscillatory and red-noise AMOC regimes indicate that North Atlantic-forced AMOC is suppressed in latter regime

Abstract

The relationship between Atlantic Meridional Overturning circulation (AMOC) variability and high-latitude North Atlantic buoyancy changes is complicated by the latter both driving, and responding to, AMOC changes. A Maximum Covariance Analysis applied to a 1201-year preindustrial control simulation reveals two leading modes that separate these two distinct roles of North Atlantic temperature and salinity as related to AMOC variability. A linear combination of the two modes accounts for most of the variation of a widely-used AMOC index. The same analysis applied to another control simulation known to possess two distinct regimes of AMOC variability - oscillatory and red-noise - suggests that the North Atlantic buoyancy-forced AMOC variability is present in both regimes but is weaker in the latter, and moreover there is pronounced multidecadal/centennial AMOC behavior in the latter regime that is unrelated to North Atlantic buoyancy forcing.

Plain Language Summary

Atlantic Meridional Overturning Circulation (AMOC) variations cause significant changes to the global climate. High latitude North Atlantic temperature and salinity variations modify the AMOC through changing the buoyancy of the upper ocean. However, this identification is complicated by the reverse relationship, that North Atlantic temperature and salinity changes with AMOC. When we apply Maximum Covariance Analysis – a spatiotemporal analysis designed to find coupled patterns between two climate fields - to a preindustrial control simulation of a fully-coupled climate model, it extracts the two coupling relationships. Moreover, the combination of these two behaviors is sufficient to characterize the AMOC variations. When we apply the same analysis method to another control simulation exhibiting two regimes of AMOC variability – oscillatory and red-noise - it reveals that the red-noise regime has a marked reduction to the AMOC variability resulting from North Atlantic buoyancy forcing, and a corresponding increase in multidecadal/centennial AMOC variations of undetermined origin.

1. Introduction

This study addresses the interconnected relationship between upper-ocean temperature and salinity in the high-latitude North Atlantic and the variability of the Atlantic Meridional Overturning circulation (AMOC) on decadal and longer timescales. A number of studies attribute changes to upper-ocean buoyancy anomalies in the high latitude North Atlantic to drive AMOC variations, the former originating through atmospheric forcing directly on deepwater formation regions (e.g. Delworth et al. 1993, Danabasoglu 2008, Kim et al. 2020), or mediated to the western boundary though advection or Rossby wave propagation (e.g. Buckley et al. 2012). Idealized simulations where a pulse buoyancy forcing is applied to the high-latitude North Atlantic supports this interpretation (Zhang and Zhang 2015; Kim et al. 2020). Many studies also argue for the reverse coupling, that the ocean heat flux convergence caused by AMOC variability drives upper-ocean temperature anomalies in the high latitude North Atlantic (e.g. Häkkinen 1999, Zhang 2008, Zhang and Zhang 2015). However, for internal AMOC variations in climate model simulations, co-mingling of the two processes means that the cause-and-effect relationship is difficult to establish.

Untangling these directional relationships is key to understanding AMOC variability (Buckley and Marshall 2016). Some have argued that the ocean dynamical response in the high-latitude North Atlantic to the AMOC variation induces a delayed feedback that alters the behavior of the AMOC, including its persistence (Kwon and Frankignoul 2012) or timescale of variation (Griffies and Tziperman 1995, Dong and Sutton 2005, Kwon and Frankignoul 2014). In contrast, others have argued that the AMOC variation is a passive response to buoyancy anomalies in the high-latitude North Atlantic (e.g. Buckley et al. 2012). Untangling these relationships also reveals the nature of the forced AMOC response to a warming climate: Tandon and Kushner (2015) found in historical model simulations that an unforced AMOC increase lead to North Atlantic sea surface temperature (SST) warming, whereas a forced warming of North Atlantic SST leads to an AMOC weakening.

There exists an objective spatiotemporal analysis technique - Maximum Covariance Analysis (MCA; Bretherton et al. 1992) – designed to extract coupled patterns between two climate fields, such as the problem described above. A lagged MCA has previously been used to reveal the two-way response of the North Atlantic atmosphere with AMOC variability (Gastineau and Frankignoul 2012). However, MCA has not been previously applied to relate

AMOC variations to North Atlantic upper-ocean temperature and salinity. Also, studies linking AMOC changes to underlying drivers or responses typically assume an index of AMOC strength to represent the totality of AMOC variations, for example the first EOF of the meridional overturning circulation (MOC) streamfunction, or the maximum value of the MOC streamfunction within the North Atlantic. The choice of index is somewhat subjective, and moreover does not allow for diversity in the spatiotemporal structure of AMOC variability. A MCA approach, on the other hand, makes no prior assumptions about the structure of AMOC variations.

In the following, we apply MCA to a control simulation of a fully coupled model to objectively extract coupled spatial patterns between AMOC and high latitude North Atlantic upper ocean temperature and salinity. We also apply the MCA to a control simulation of another model that exhibits two regimes of AMOC behavior, oscillatory and red-noise, to examine what the method reveals about the nature of the two regimes.

2. Materials and Methods

We use years 1000-2200 of a preindustrial (1850) control run of the Community Earth System Model version 1.2 (CESM1) at 1° horizontal resolution as described in Kay et al. (2015) (years 1-1000 shows a downward trend in the AMOC strength). We also use a T85 simulation of the Community Climate System Model version 3 (hereafter CCSM T85) that has been extensively analyzed for AMOC specifically its regime shift (Danabasoglu 2008, Danabasoglu et al. 2012, Kwon and Frankignoul 2012 and 2014). We also use a set of idealized CESM1 simulations where a pulse buoyancy forcing designed to mimic the effect of a boreal winter (Dec-March) NAO event was applied to the Labrador Sea to examine its effect on the AMOC. The runs are the same as in Kim et al. (2020). A heat flux anomaly was applied over 10 years to the Labrador Sea domain 50-64°N and 45-61°W representative of a North Atlantic Oscillation (NAO) event; a set of 10 ensemble members were run with positive values of the anomaly, and another 10 with negative values. The reader is referred to Kim et al. (2020) for simulation details.

Maximum Covariance Analysis (MCA) is used to extract coupled patterns relating AMOC to North Atlantic upper ocean temperature and salinity, following Bretherton et al. (1992). For the left field, we use the annual mean MOC streamfunction anomalies in the Atlantic. That data is first interpolated (using bilinear interpolation) onto an equally-spaced

latitude and depth grid, from 33.5°S to 65.5°N in intervals of 1°, and from 50m to 4950m in steps of 100m. The data is then detrended and light temporal smoothing (5-year running mean) is applied to remove the interannual variation. For the right field, we use the annual mean temperature and salinity anomalies averaged over the top 1000m for the North Atlantic north of 40°N; the data is left on the native ocean model horizontal grid. The temperature and salinity anomalies are converted to their density equivalents, multiplied by the square root of the grid area, and the resulting data combined to form a single field. A cross-covariance matrix is formed using the left and right fields, and a singular value decomposition is applied to solve for the MCA modes. The first two modes account for over 90% of the cumulative squared covariance fraction (supplementary figure S1); our analysis focuses on these two modes. In subsequent analysis, the spatial patterns shown are homogeneous regression maps, calculated by regressing the field of interest onto the normalized expansion coefficient. Regression slopes are only plotted if the associated correlation coefficient is significantly different from zero. Significance of correlations is assessed using the t-statistic and with the effective sample size calculated using equation 2 of Ebisuzaki (1997).

3. MCA analysis on CESM1

Figure 1a and figure S2a shows the MOC spatial pattern and expansion coefficients associated with mode 1, respectively. It is characterized by an interhemispheric AMOC increase, associated with warmer and saltier waters in the high latitude North Atlantic by the Irminger and Labrador seas (figure 1c, d). The associated density changes (figure 1e) are largely negative but small, indicating compensation between the temperature and salinity changes. The variation for both the MOC and temperature/salinity (hereafter T/S) expansion coefficients are dominated by lower frequencies between 25 to 250-year period (figure S2c and d, blue lines). Lag correlation between the MOC and T/S expansion coefficients show that the MOC expansion coefficients lead that for T/S by 1-3 years (figure S2e). They suggest that the temperature and salinity patterns seen in figure 1c, d are a consequence of the AMOC strengthening.

Figure 1b and figure S2b shows the MOC spatial pattern and expansion coefficients associated with mode 2, respectively. It is characterized by an AMOC increase limited to the mid and high latitude North Atlantic and associated with colder and fresher upper ocean waters

there (figure 1f, g) and density increase near the Irminger and Labrador seas (figure 1h). The variation for the MOC expansion coefficients peak between 20-to-50-year period (figure S2c, red line), whereas the T/S expansion coefficients peak possess a broader spectrum (figure S2d, red line). For the MOC (left) expansion coefficients (figure S2c), mode 1 has generally lower frequencies but there is an overlap between mode 1 and mode 2 between around 0.025/yr and 0.04/yr. Lag correlation between the MOC and T/S expansion coefficients show that the latter leads the former by 1 year (figure S2f). The results suggest that this mode represents the AMOC responding to increase in North Atlantic upper ocean density from cooler ocean temperatures.

As a check to see whether temperature or salinity dominates the MCA result, the MCA was repeated using each field individually. In each case, the MCA mode 1 and 2 spatial patterns closely resembled those for the MCA with both temperature and salinity (figure not shown). Moreover, the correlation between the mode 1 MOC expansion coefficients for the MCA with only temperature or salinity, with the full MCA, is high ($r > 0.94$ in both cases); and similarly for mode 2. Thus, both temperature and salinity contribute to the MCA result.

To check the temporal relationships inferred from the MCA analysis, we repeated the MCA but with a temporal shift applied to the T/S field relative to the MOC field (Czaja and Frankignoul 1999, Gastineau and Frankignoul 2012). The assumption is that the squared covariance explained for the mode of interest will be maximized when the lag reflects the physical coupling extracted. The results are consistent with the lead/lag relationship between MOC and T/S for modes 1 and 2 stated above. The squared covariance fraction for mode 1 is maximized when MOC leads T/S by 5 years (figure S3, blue bars). The MOC expansion coefficients at this lag correlate with mode 1 for our original MCA (zero lag) at $r = 0.976$, meaning that they represent the same physical process. For mode 2, the squared covariance fraction maximizes when MOC lags T/S by 1 year, and the left expansion coefficients for this mode at this lag correlates with mode 2 for our original MCA (zero lag) at $r = 0.984$. We revert to the original (i.e., unlagged) MCA modes for the subsequent discussion.

Modes 1 and 2 are curious as the temperature and salinity changes appear to be diametrically opposite: mode 1 associates an AMOC increase with a warmer and saltier high latitude North Atlantic, whereas mode 2 associates an AMOC increase (albeit at high latitudes) with a colder and fresher high latitude North Atlantic. We interpret the two modes to represent two different stages of the AMOC variation: mode 2 shows the initial response of the AMOC to

colder and denser high latitude North Atlantic waters, whereas mode 1 shows the subsequent evolution where the AMOC strengthening extends southwards, and the resulting ocean circulation change leads to a warmer and saltier high latitude North Atlantic.

Two pieces of evidence support this interpretation. First, a lag correlation between the MOC expansion coefficients for the two modes (figure 2a) shows that they are significantly correlated, and that peak correlation (r = 0.64) occurs when mode 2 leads mode 1 by 2-3 years; in other words, the high-latitude MOC increase (figure 1b) precedes the interhemispheric MOC increase (figure 1a). Second, an idealized simulation with an NAO-like density perturbation in the North Atlantic using the same CESM1 model (Kim et al. 2020; see section 2) shows the evolution of the MOC from one restricted to the high latitude North Atlantic in the first few years, to a more interhemispheric pattern in the second decade of its evolution (figure 2b). The initial MOC perturbation resembles the MCA mode 2 pattern (figure 1b), whereas the later MOC perturbation resembles the MCA mode 1 pattern (figure 1a). A similar MOC evolution to a pulse-like NAO buoyancy forcing is seen in the GFDL CM2.1 (Delworth and Zeng 2016). This interpretation is also consistent with the evolution of AMOC anomalies found in many previous studies (e.g., Biastoch et al. 2008, Deshayes and Frankignoul 2008, Kwon and Frankignoul 2014, Zhang and Zhang 2015).

The MCA thus decomposes the AMOC variability into two modes, each with its own spatial pattern and temporal behavior. How do they relate to traditional indices of AMOC variability? We compare the MOC expansion coefficients to a standard index for the AMOC, namely the maximum AMOC streamfunction value (below 500m depth) at a given latitude. Using this AMOC index at 47.5°N, we find that a multivariate linear regression using the modes 1 and 2 MOC expansion coefficients (over the entire 1201 years) as predictors provides a good fit, but with most of the fit coming from mode 2 (the high latitude AMOC pattern) (figure S4, left panels). On the other hand, for the AMOC index at 37.5°N the linear combination again provides a good fit but with most of it coming from mode 1, the interhemispheric MOC pattern (figure S4, right panels). The same comparison for each latitude between 20-50°N (figure 3) reveals that the two MOC expansion coefficients are consistently able to account for most of the variance (>70%) of the AMOC index except for a narrow band between 33-34°N (figure 3b). Mode 2 essentially represents the AMOC maximum streamfunction value at higher latitudes, and mode 1 represents the AMOC maximum streamfunction value for lower latitudes,

with 42.5°N being the threshold latitude (figure 3a). Thus, the two MCA modes encompasses the span of behaviors represented by the AMOC maximum streamfunction index at almost all latitudes of interest between 20-50°N. We speculate that the poor fit between 33-34°N arises because the MCA analysis does not capture wind-driven MOC variations that contribute substantially to AMOC variation in the midlatitudes (Biastoch et al. 2008, Larson et al. 2020).

4. Analysis of the CCSM3 T85 AMOC regime shift

We apply the MCA decomposition to a 699-year CCSM3 T85 simulation that has previously been shown to exhibit two distinct regimes of AMOC variability: an oscillatory regime with pronounced quasi-periodic behavior of ~20yrs over years 150-399 (hereafter **regime I**), and a multidecadal/centennial red-noise like behavior over years 450-699 (hereafter **regime II**) (Danabasoglu et al. 2012, Kwon and Frankignoul 2014) (figure S5). We explore whether the MCA method reveals useful information about the nature of the two regimes. Applying the MCA analysis over years 150-699 reveals that the first two modes dominate, possessing properties qualitatively like the MCA modes 1 and 2 derived for the CESM1 respectively (figure S6 and S7). As a check, we repeated the MCA for each regime separately; for each instance, the modes 1and 2 obtained possess similar properties to that for the MCA analysis over years 150-699 (not shown).

The regime change in the AMOC is expressed differently in the two modes. Mode 1 is expressed as a timescale change, from quasi-periodic behavior in regime 1 to a pronounced multidecadal/centennial variation in regime 2 (figure 4a, blue line); this difference is also expressed in the power spectrum for mode 1 MOC expansion coefficients for each regime (figures S6c and d, blue lines). The amplitude of variation of mode 1 is comparably large in both regimes. On the other hand, the regime change in mode 2 is expressed primarily in terms of amplitude, with regime I showing a larger amplitude of variation (figure 4a and figure S6c and d, red line). Regime II is also more irregular and less periodic than regime I, as inferred from the power spectrum for mode 2 MOC expansion coefficients for each regime (figures S6c and d, red line).

The temporal relationship between modes 1 and 2 also appears to differ between the two regimes. In regime I, the MOC expansion coefficients for mode 2 is correlated to that for mode 1 at r = 0.71 with a 4-year lag (mode 1 lags mode 2); this is qualitatively like the relationship

seen in the CESM1 (figure 2a). On the other hand, for regime II, mode 2 is not as strongly correlated with mode 1: the best lead/lag relationship is r = 0.45 with a 3-year lag. However, a stronger lead/lag relationship between the two MCA modes for regime II is recovered if we consider only the shorter timescale variations corresponding to the oscillatory behavior. We use Ensemble Empirical Mode Decomposition (EEMD; Huang et al. 1998, Wu and Huang 2009) to filter the MCA expansion coefficients into shorter decadal (periods less than ~64 years) and longer multidecadal/centennial timescales, by using the sum of EEMD intrinsic mode functions (IMFs) 1-4 for the former and EEMD IMFs 5-10 for the latter (figure 4b and c, respectively) (see supplementary information section S2 for details). When we repeat the lag correlation but for decadal timescale variations, for regime I we get r = 0.77 for when MCA mode 2 leads mode 1 by 4 years. For regime II, we get r = 0.61 when mode 2 leads mode 1 by 3 years (figure 4b); in other words, we recover the relationship between mode 2 and 1 for these timescales. For the longer multidecadal/centennial timescales, mode 2 has little to no longer-term variation to speak of, and the two modes are clearly unrelated (figure 4c). This suggests that the longer timescale interhemispheric AMOC behavior has origins independent of high latitude North Atlantic buoyancy forcing.

We conclude that the high latitude North Atlantic buoyancy driving of AMOC variability (mode 2) is present in both regimes, albeit weaker in the latter. Kwon and Frankignoul (2014) notes that there is increased densification of the deep ocean (2000-3000m) in regime 2 relative to regime 1, and this may be the reason why regime II has a more muted variation because of the presence of a more stable vertical stratification. On the other hand, the multidecadal/centennial timescale AMOC variability resides almost exclusively in the interhemispheric AMOC response (mode 1) and is strongly expressed in regime II but not regime I (figure 4c).

5. Summary and Discussion

We examine the relationship between AMOC variability with high latitude upper ocean North Atlantic temperature and salinity using a Maximum Covariance Analysis designed to extract coupled modes of variability between the two climate fields. The first two modes explain over 90% of the cumulative squared covariance fraction. Mode 1 possesses an interhemispheric increase in AMOC coupled to a warmer and saltier North Atlantic, and with the MOC expansion coefficients leading the T/S expansion coefficients by 2-3 years. Mode 2 possesses a high-

latitude North Atlantic AMOC increase coupled to a colder and fresher high latitude North Atlantic, qualitatively opposite to mode 1. The two modes represent different phases of AMOC variability driven by buoyancy forcing in the high-latitude North Atlantic: colder SSTs in the high latitude North Atlantic increases the high-latitude AMOC, which then evolves into an interhemispheric AMOC increase. The resulting AMOC increase leads to ocean circulation changes that bring warmer and saltier upper ocean water to the high latitude North Atlantic. This mechanism for AMOC variation has been noted before (e.g., Kwon and Frankignoul 2014), but the novelty of our result is that the MCA objectively extracts the two distinct couplings.

Our analysis of the two previously-identified AMOC regimes – oscillatory and red-noise - of the CCSM3 T85 simulation (Danabasoglu et al. 2012, Kwon and Frankignoul 2014) suggests that the North Atlantic buoyancy-driven AMOC variability operates at shorter decadal timescales and for both regimes, albeit suppressed in the latter. Moreover, the longer multidecadal/centennial AMOC variability is expressed only in the interhemispheric AMOC (mode 1) and is especially pronounced in the red-noise regime. We conclude that the two regimes arise because (i) the North Atlantic buoyancy-forced AMOC variation is suppressed in the red-noise regime, and (ii) the multidecadal/centennial interhemispheric AMOC variation, unrelated to North Atlantic buoyancy forcing, is especially pronounced in the red-noise regime.

Our inferred mechanism for AMOC decadal variability suggests a delayed negative feedback, since a colder high latitude North Atlantic that starts off the AMOC perturbation ultimately leads to warmer conditions there several years later. A similar feedback was suggested by Kwon and Frankignoul (2014) to explain the 20-year oscillation in regime I of the CCSM3 T85. Why the oscillation manifests itself more strongly in regime I remains an open question, though our analysis suggests that high-latitude North Atlantic buoyancy forcing is less able to excite an AMOC response in regime II, possibly because of the increased vertical stability. Idealized simulations that examine the transient AMOC response to density perturbations under different mean vertical stratification may shed light on this question.

Acknowledgments, Samples, and Data

We thank Young-Oh Kwon for providing the MOC streamfunction for the CCSM T85, and Steve Yeager, Gohkan Danabasoglu, Wilber Weijer, and Jiaxu Zhang for useful discussions. This research is supported by the National Oceanic and Atmospheric Administration Climate Program Office under Climate Variability and Predictability Program

grants NA16OAR4310169, NA16OAR4310170, NA16OAR4310171; Regional and Global Climate Modeling Program (RGCM) of the U.S. Department of Energy's (DOE) Office of Science (BER) through support of the HiLAT project; and by the National Science Foundation (NSF) Collaborative Research EaSM2 grant OCE-1243015. NCAR is sponsored by the NSF under Cooperative Agreement 1852977. Computing resources were provided by the Climate Simulation Laboratory at NCAR's Computational and Information Systems Laboratory, sponsored by the NSF. The NSF and DOE BER RGCM support the CESM project. This is UW/CICOES contribution 2020-1134, and PMEL contribution 5238.

No new data was generated for this work. The CESM1 preindustrial simulation is available at doi:10.5065/d6j101d1 (Kay and Deser 2016). The CCSM T85 simulation is available from the Climate Data Gateway at the National Center for Atmospheric Research (https://www.earthsystemgrid.org), simulation b30.009. We also utilized Matlab scripts developed by Daniel Vimont (https://www.aos.wisc.edu/~dvimont/matlab).

References

Bretherton, C.S., Smith, C. and Wallace, J.M., 1992. An intercomparison of methods for finding coupled patterns in climate data. *Journal of climate*, *5*(6), pp.541-560.

Biastoch, A., Böning, C.W., Getzlaff, J., Molines, J.M. and Madec, G., 2008. Causes of interannual–decadal variability in the meridional overturning circulation of the midlatitude North Atlantic Ocean. *Journal of climate*, *21*(24), pp.6599-6615.

Buckley, M.W., Ferreira, D., Campin, J.M., Marshall, J. and Tulloch, R., 2012. On the relationship between decadal buoyancy anomalies and variability of the Atlantic meridional overturning circulation. *Journal of climate*, *25*(23), pp.8009-8030.

Buckley, M.W. and Marshall, J., 2016. Observations, inferences, and mechanisms of the Atlantic Meridional Overturning Circulation: A review. *Reviews of Geophysics*, *54*(1), pp.5-63.

Danabasoglu, G., 2008. On multidecadal variability of the Atlantic meridional overturning circulation in the Community Climate System Model version 3. *Journal of Climate*, *21*(21), pp.5524-5544.

Danabasoglu, G., Yeager, S.G., Kwon, Y.O., Tribbia, J.J., Phillips, A.S. and Hurrell, J.W., 2012. Variability of the Atlantic meridional overturning circulation in CCSM4. *Journal of climate*, *25*(15), pp.5153-5172.

Delworth, T., Manabe, S. and Stouffer, R.J., 1993. Interdecadal variations of the thermohaline circulation in a coupled ocean-atmosphere model. *Journal of Climate*, *6*(11), pp.1993-2011.

Delworth, T.L. and Zeng, F., 2016. The impact of the North Atlantic Oscillation on climate through its influence on the Atlantic meridional overturning circulation. *Journal of Climate*, *29*(3), pp.941-962.

Deshayes, J., and C.F. Frankignoul, 2008: Simulated variability of the circulation in the North Atlantic from 1953 to 2003. J. Climate, 21, 4919-4933.

Dong, B. and Sutton, R.T., 2005. Mechanism of interdecadal thermohaline circulation variability in a coupled ocean–atmosphere GCM. *Journal of climate*, *18*(8), pp.1117-1135.

Ebisuzaki, W., 1997. A method to estimate the statistical significance of a correlation when the data are serially correlated. *Journal of Climate*, *10*(9), pp.2147-2153.

Gastineau, G., and C. Frankignoul, 2012: Cold-season atmospheric response to the natural variability of the Atlantic meridional overturning circulation. Climate Dyn., 39, 37-57.

Griffies, S.M. and Tziperman, E., 1995. A linear thermohaline oscillator driven by stochastic atmospheric forcing. *Journal of Climate*, *8*(10), pp.2440-2453.

Häkkinen, S., 1999. Variability of the simulated meridional heat transport in the North Atlantic for the period 1951–1993. *Journal of Geophysical Research: Oceans*, *104*(C5), pp.10991-11007.

Huang, N.E., Shen, Z., Long, S.R., Wu, M.C., Shih, H.H., Zheng, Q., Yen, N.C., Tung, C.C. and Liu, H.H., 1998. The empirical mode decomposition and the Hilbert spectrum for nonlinear and non-stationary time series analysis. *Proceedings of the Royal Society of London. Series A: mathematical, physical and engineering sciences*, *454*(1971), pp.903-995.

Kay, J.E., Deser, C., Phillips, A., Mai, A., Hannay, C., Strand, G., Arblaster, J.M., Bates, S.C., Danabasoglu, G., Edwards, J. and Holland, M., 2015. The Community Earth System Model (CESM) large ensemble project: A community resource for studying climate change in the presence of internal climate variability. *Bulletin of the American Meteorological Society*, *96*(8), pp.1333-1349.

Kay, J. and Deser, C. (2016). "The Community Earth System Model (CESM) Large Ensemble Project" UCAR/NCAR Climate Data Gateway. DOI:10.5065/d6j101d1

Kim, W.M., Yeager, S. and Danabasoglu, G., 2020. Atlantic Multidecadal Variability and Associated Climate Impacts Initiated by Ocean Thermohaline Dynamics. *Journal of Climate*, *33*(4), pp.1317-1334.

Kwon, Y.O. and Frankignoul, C., 2012. Stochastically-driven multidecadal variability of the Atlantic meridional overturning circulation in CCSM3. *Climate dynamics*, *38*(5-6), pp.859-876.

Kwon, Y.O. and Frankignoul, C., 2014. Mechanisms of multidecadal Atlantic meridional overturning circulation variability diagnosed in depth versus density space. *Journal of Climate*, *27*(24), pp.9359-9376.

Larson, S.M., Buckley, M.W. and Clement, A.C., 2020. Extracting the Buoyancy-Driven Atlantic Meridional Overturning Circulation. *Journal of Climate*, *33*(11), pp.4697-4714.

Tandon, N.F. and Kushner, P.J., 2015. Does external forcing interfere with the AMOC's influence on North Atlantic sea surface temperature? *Journal of Climate*, *28*(16), pp.6309-6323.

Wu, Z. and Huang, N.E., 2009. Ensemble empirical mode decomposition: a noise-assisted data analysis method. *Advances in adaptive data analysis*, *1*(01), pp.1-41.

Zhang, R., 2008. Coherent surface-subsurface fingerprint of the Atlantic meridional overturning circulation. *Geophysical Research Letters*, *35*(20).

Zhang, J. and Zhang, R., 2015. On the evolution of Atlantic meridional overturning circulation fingerprint and implications for decadal predictability in the North Atlantic. Geophysical Research Letters, 42(13), pp.5419-5426.

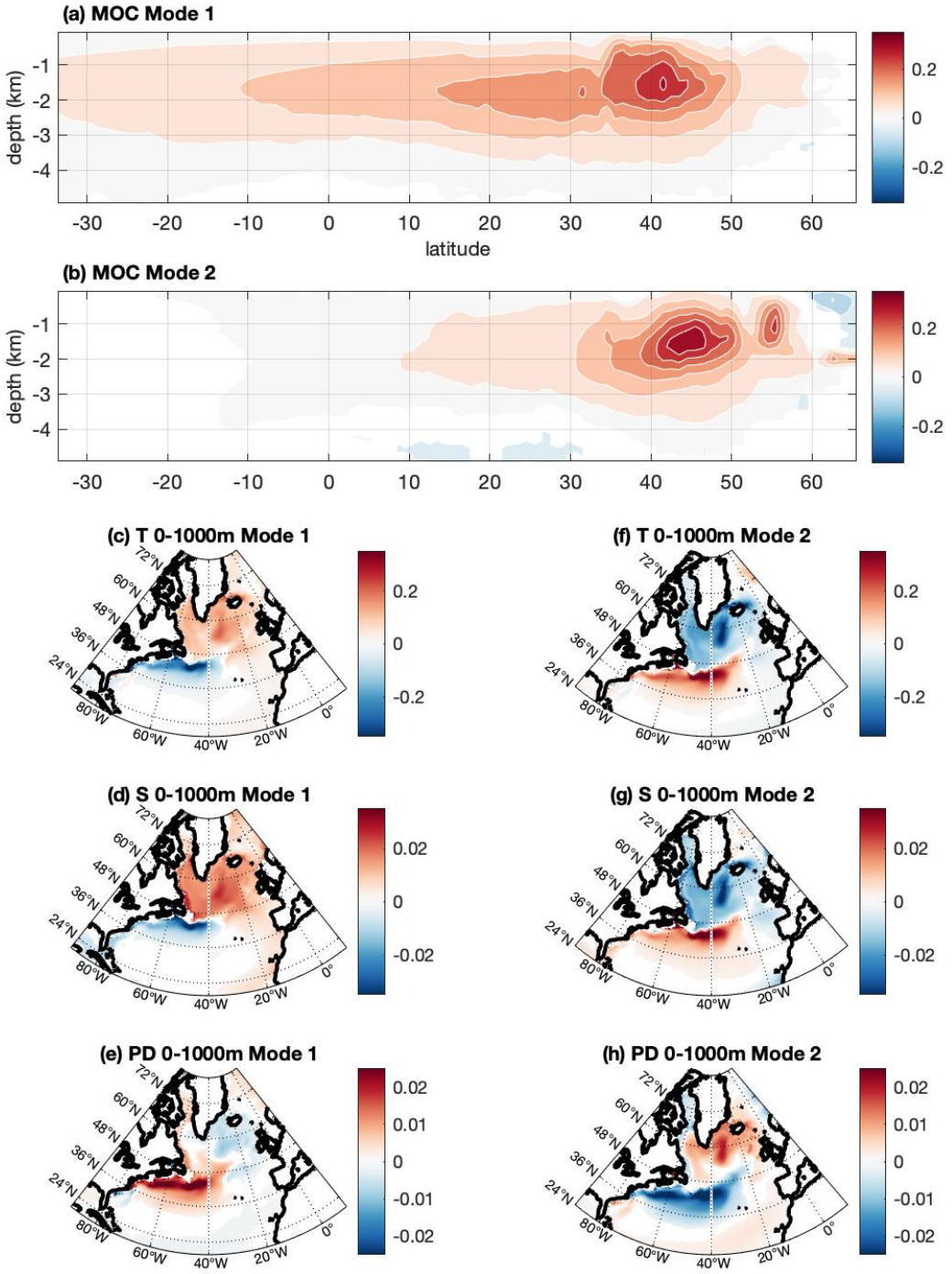

Figure 1. MCA on CESM1. **(a)** Homogeneous regression map onto mode 1 MOC expansion coefficients. **(b)** Same as (a), for mode 2. **(c-e)** Regression maps of 0-1000m averaged (c) temperature, (d) salinity, and (e) density onto mode 1 T/S expansion coefficients. **(f-h)** Same as (c-e), for mode 2. Values are shown only where the correlation is significant ($p < 0.05$).

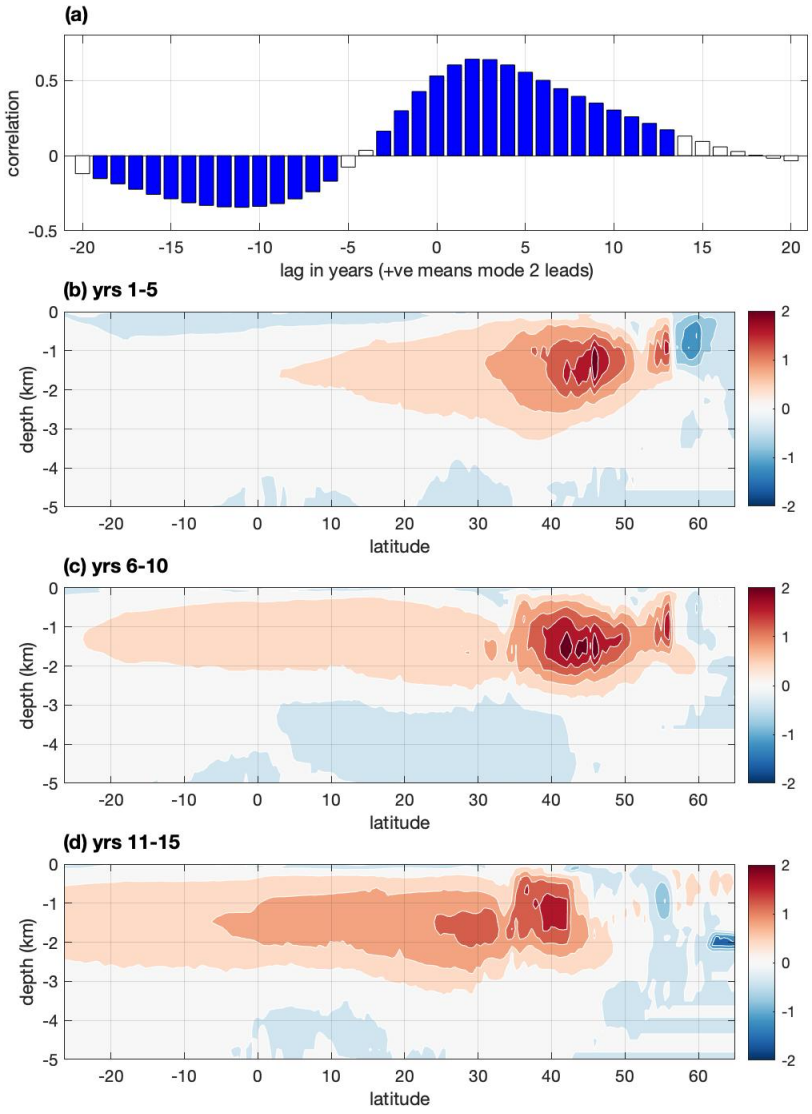

Figure 2. (a) Lag correlation between mode 1 and 2 MOC expansion coefficients. Significant correlations ($p < 0.05$) are indicated by filled bars. **(b-d)** CESM1 transient AMOC response to an imposed pulse buoyancy flux anomaly over the Labrador Sea. The years indicated correspond to the average of years after onset of the forcing. Contour interval is 0.4Sv.

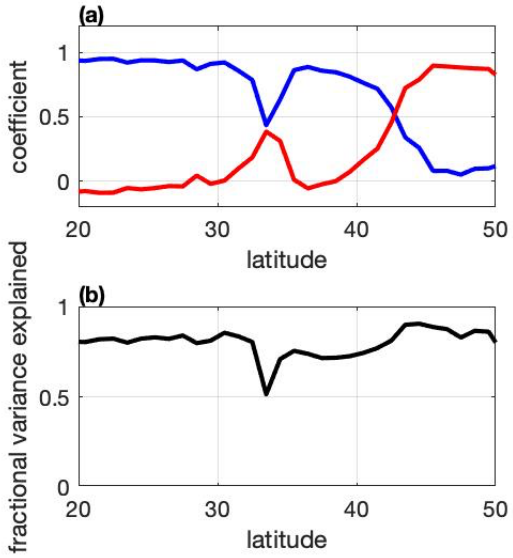

Figure 3. Multivariate regression of mode 1 and 2 MOC expansion coefficients with the AMOC maximum streamfunction at the given latitude, over the entire 1201 years. **(a)** Regression coefficient as a function of latitude for mode 1 (blue) and 2 (red). **(b)** Fractional variance explained of the AMOC maximum streamfunction by the best-fit linear sum of modes 1 and 2.

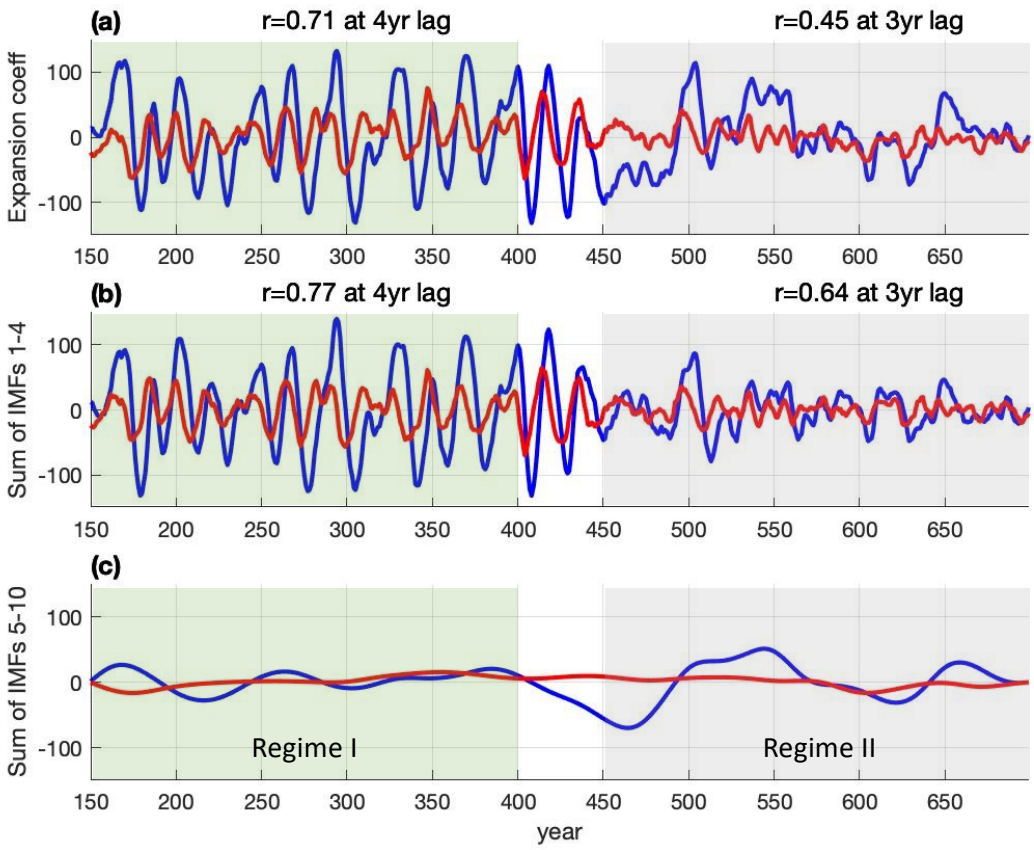

Figure 4. MCA on CCSM T85. **(a)** MOC expansion coefficients. **(b-c)** Expansion coefficients filtered for (b) shorter (sum of EEMD IMFs 1-4) and (c) longer timescales (sum of IMFs 5-10). Mode 1 is in blue, and 2 in red. Indicated in (a) and (b) are the maximum lead/lag correlation between mode 1 and 2 for each regime, with mode 1 lagging mode 2 by the years indicated.